Electronic Supplementary Information

Building block magneto-luminescent nanomaterials of iron-oxide@ZnS@LaF_3:Ce^{3+},Gd^{3+},Tb^{3+} with green emission

Navadeep Shrivastava,[ab] L. U. Khan,[b] Z U. Khan,[c] J. M. Vargas,[d] O. Moscoso-Londoño,[e] Carlos Ospina,[f] H. F. Brito,[b] Yasir Javed,[g] M. C. F. C. Felinto,[h] A. S. Menezes,[a] Marcelo Knobel,[ef] S. K. Sharma*[a]

Email* - *surender76@gmail.com*

[a]*Department of Physics, Federal University of Maranhão, Av. dos Portugueses, 1966 - Bacanga, São Luís - MA, 65080-805, Brazil.*
[b]*Department of Fundamental Chemistry, Institute of Chemistry, University of São Paulo, Av. Prof. Lineu Prestes, 748, 05508-000, São Paulo-SP, Brazil.*
[c]*Department of Immunology, Institute of Biomedical Sciences-IV, University of São Paulo, Av. Prof. Lineu Prestes, 1730, 05508-000 São Paulo-SP, Brazil.*

[d]*Consejo Nacional de Investigaciones Científicas y Técnicas (CONICET), Centro Atómico Bariloche, Av. Bustillo 9500, 8400, San Carlos de Bariloche, Rıo Negro, Argentina*

[e]*Institute of Physics "Gleb Wataghin", State University of Campinas (UNICAMP), 13083-859, Campinas- SP, Brazil.*
[f]*Brazilian Nanotechnology National Laboratory (LNNano–CNPEM), Rua Giuseppe Máximo Scolfaro 10000, 13083-100, Campinas, São Paulo, Brazil.*
[g]*Department of Physics, University of Agriculture, Faisalabad, Pakistan.*
[h]*Nuclear and Energy Research Institute - IPEN, University of Sao Paulo ,Av. Prof. Lineu Prestes, 2242 - SP, 05508-000 São Paulo-SP, Brazil.*

S1: Transmission Electron Microscopy and Electron Dispersive Spectroscopy

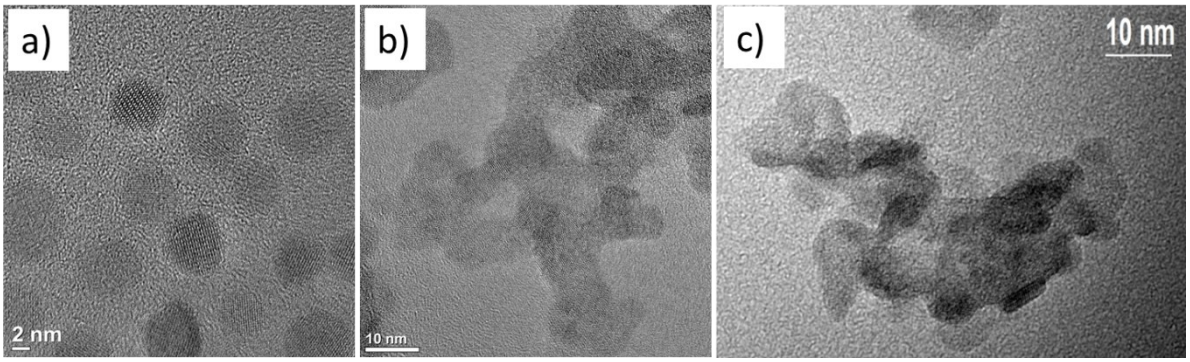

Fig. S1-A: High resolution transmission electron microscopy (HRTEM) images of (a) Fe_3O_4, (b) Fe_3O_4/ZnS@LaF_3:xCe^{3+},xGd^{3+},yTb^{3+} (x = 5, y = 5 mol.%) and (c) Fe_3O_4/ZnS@LaF_3:xCe^{3+},xGd^{3+},yTb^{3+} (x = 5, y = 10 mol.%), showing different mass-thickness contrast of the materials.

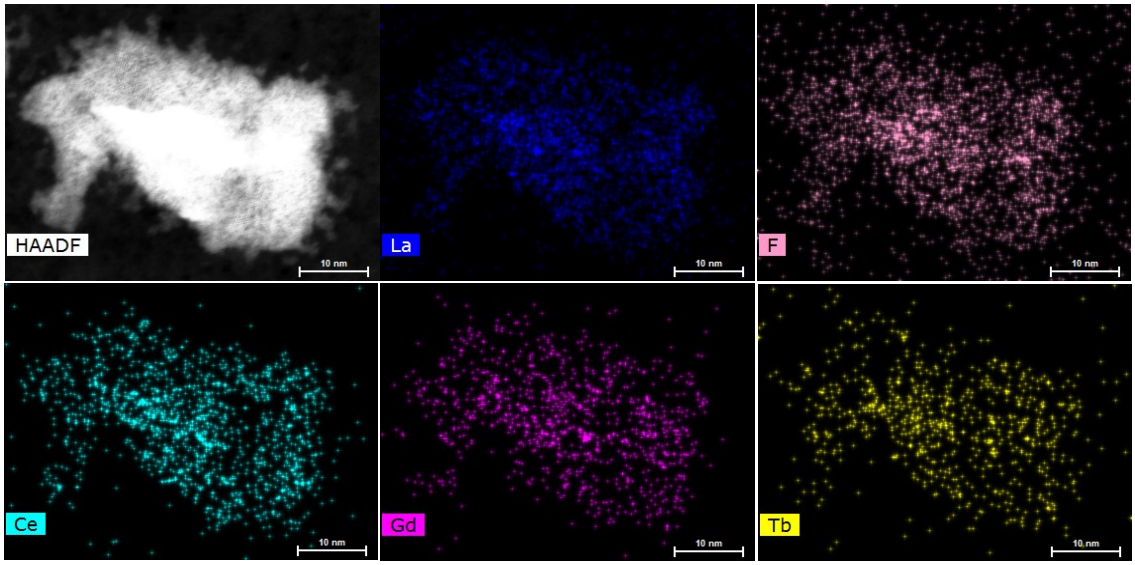

Fig. S1-B: High-Angle Annular Dark-Field (HAADF) image and EDS elemental mappings, acquired in the Titan Cubed Themis 300 microscope, showing the homogeneous and uniform distribution La, F, Ce, Gd and Tb elements in sample of Fe_3O_4/ZnS@LaF_3:xCe^{3+},xGd^{3+},yTb^{3+} (x = y = 5 mol.%) nanocomposite.

EDS spectra for Fe_3O_4/ZnS@LaF_3:xCe^{3+},xGd^{3+},yTb^{3+} (x = y = 5 mol.%) sample have been acquired for three different spots/frames (1, 2 and 3). The electron beam was focused on agglomerate particles. The observed peaks confirm the existence of Fe, O, Zn, S, La, F, Ce, Gd and Tb elements. The Cu and C peaks may be due to copper grids of ultrathin carbon film with Lacey carbon.

The quantitative analysis of the mappings of the analyzed samples shows a difference in relation to a theoretical stoichiometry. In fact, the EDS analysis is a local measure of a small number of clusters observed in the image and may represent unreliable stoichiometry.

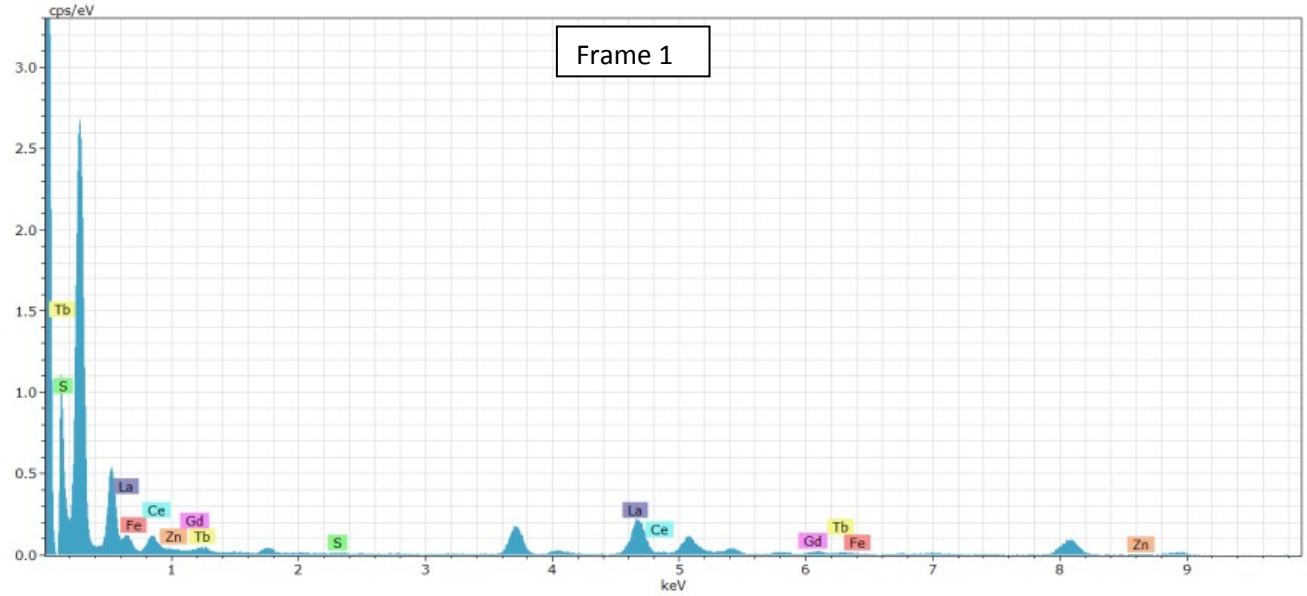

Fig. S1-C(i) EDS spectrum for Fe_3O_4/ZnS@LaF_3:xCe^{3+},xGd^{3+},yTb^{3+} (x = y = 5 mol.%) sample for spot/Frame 1.

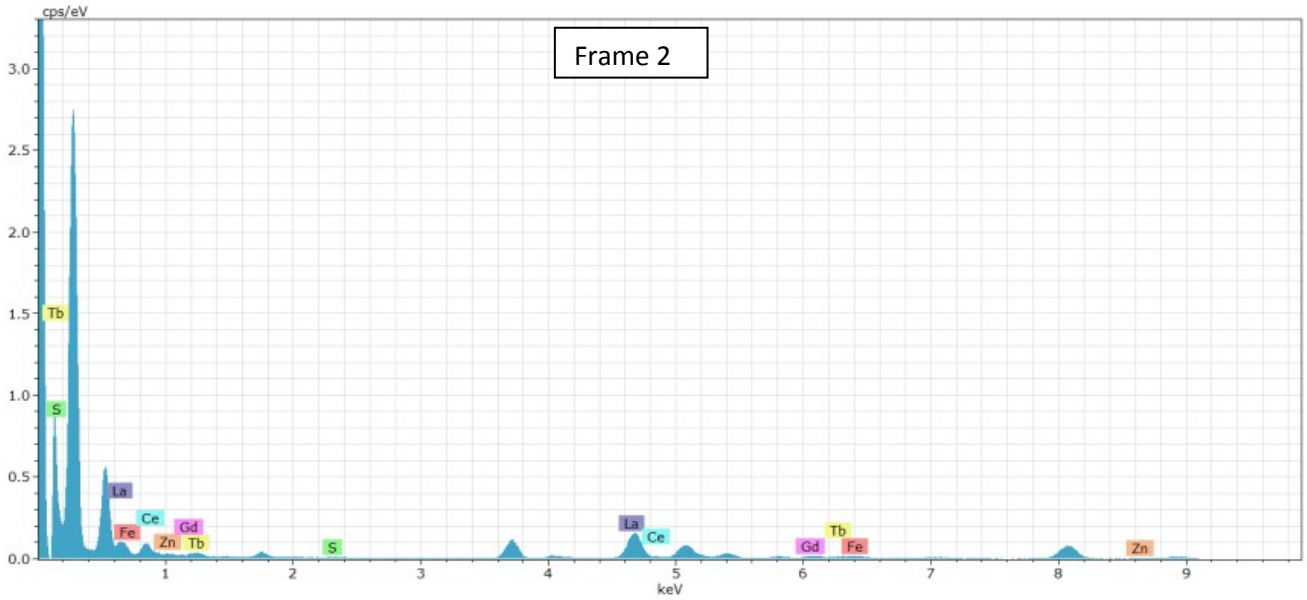

Fig. S1-C(ii) EDS spectrum for Fe_3O_4/ZnS@LaF_3:xCe^{3+},xGd^{3+},yTb^{3+} (x = y = 5 mol.%) sample for spot/Frame 2.

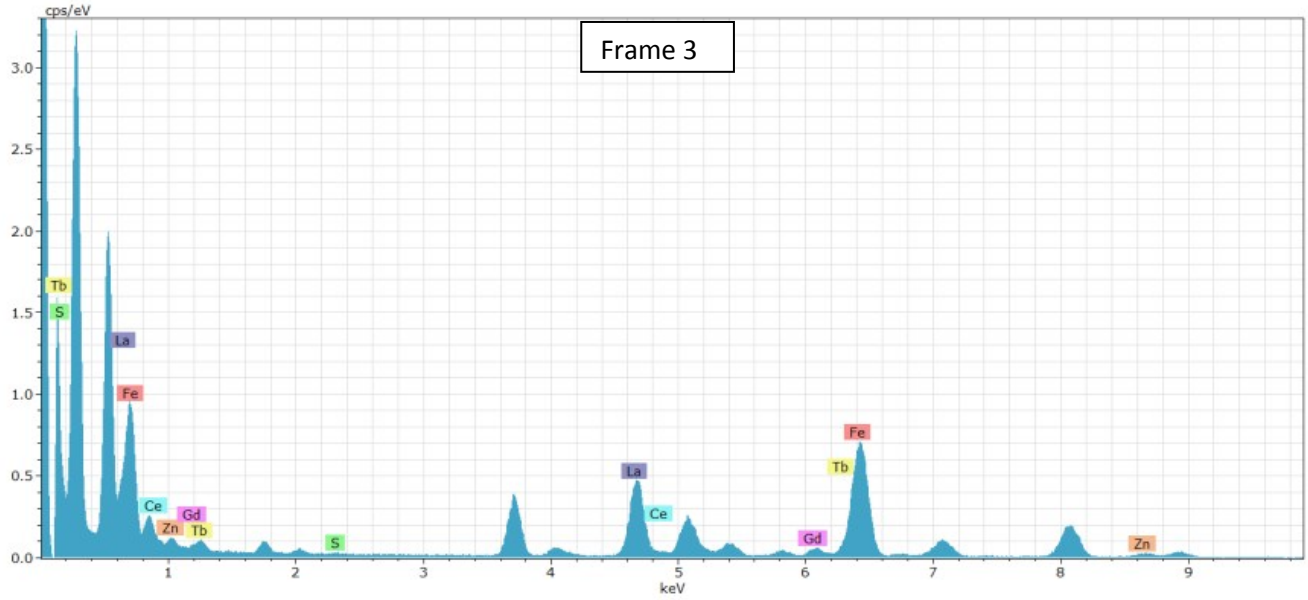

Fig. S1-C(iii) EDS spectrum for Fe_3O_4/ZnS@LaF_3:xCe^{3+},xGd^{3+},yTb^{3+} (x = y = 5 mol.%) sample for spot/Frame 3.

S2: Photoluminescence Study

It was observed that the excitation and emission spectra of reference sample LaF_3:xCe^{3+},xGd^{3+},yTb^{3+} showed same spectral features as for the magneto-luminescent Fe_3O_4/ZnS@LaF_3:xCe^{3+},xGd^{3+},yTb^{3+} nanocomposites.

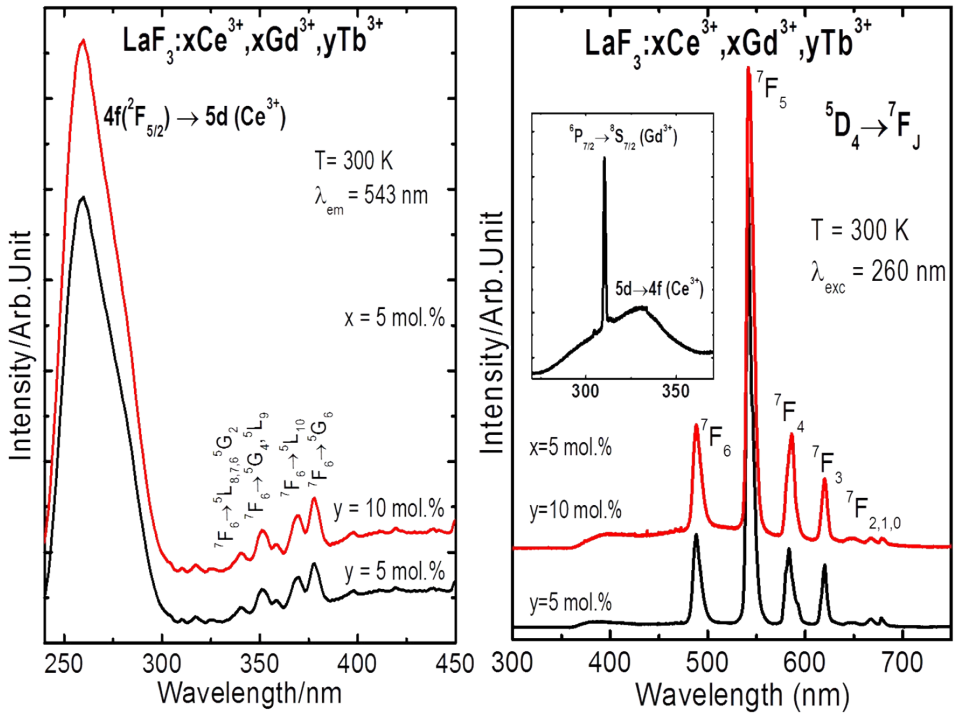

Fig. S2: Luminescence spectra of the LaF_3:xCe^{3+},xGd^{3+},yTb^{3+} (x = 5, y = 5 and 10 mol.%) nanophosphors, at room temperature (300 K): excitation spectra (left panel), monitoring emission at 543 nm assigned to the $^5D_4 \rightarrow {}^7F_5$ transition and emission spectra (right panel) under excitation at 258 nm which corresponds to the $4f(^2F_{5/2}) \rightarrow 5d$ interconfigurational transition of the Ce^{3+}. Inset figure shows the amplified spectral range of the Ce^{3+} and Gd^{3+} transition.

S3: Magnetic Study

The saturation magnetization for Fe_3O_4 and Fe_3O_4/ZnS was found 47.50 and 44.01 emu/g, respectively at 5 K (Fig. S3-A). The functionalization of semiconducting material ZnS with iron oxide did not affect magnetic property much. The higher value of saturation magnetization M_s compared to the values at 300 K, showed the dominant ferromagnetic nature of iron oxide with probably some complex interaction among ions of Fe_3O_4/ZnS nanostructure and size-shape of the nanocomposites, produced during synthesis. After coating LaF_3:xCe^{3+}, xGd^{3+}, yTb^{3+} (x =5; y = 5, 10 and 15 mol.%) around Fe_3O_4/ZnS, saturation magnetization also increased to 36.42 , 38.54 and 39.63 emu/ g for x=5 and y = 5, 10 and 15 mol.% respectively in comparison to values at room temperature (Fig S3-A). Furthermore, increasing the concentration of Tb^{3+} ions in LaF_3:xCe^{3+}, xGd^{3+},yTb^{3+} showed a small magnetic contribution of Tb^{3+} ion with variation in the coercivity value. This type of effect certainly indicated that their individual magnetic moment remained in a random fixed orientation without spontaneous magnetization switching i.e. they showed blocked regime behavior at low temperature.

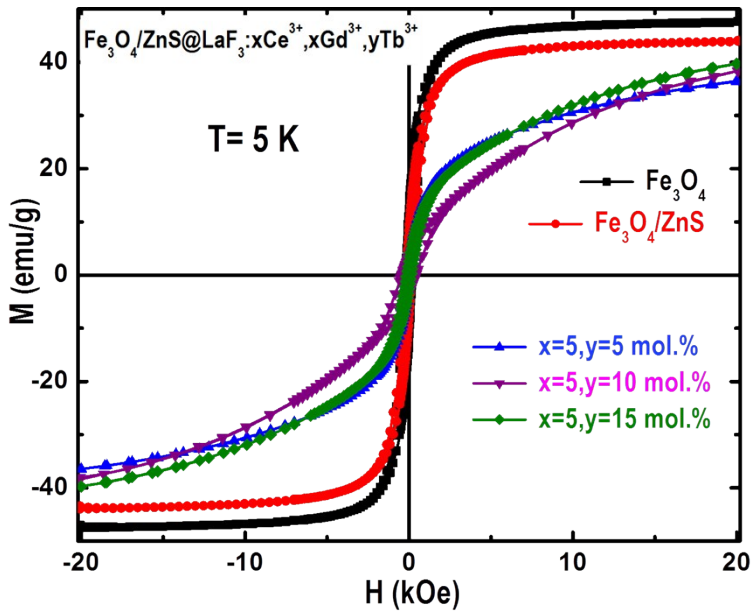

Fig. S3-A Magnetization per gram of iron oxide as a function of magnetic field for Fe_3O_4; Fe_3O_4/ZnS; and Fe_3O_4/ZnS@LaF_3:xCe^{3+},xGd^{3+},yTb^{3+} (x = 5; y = 5, 10 and 15 mol.%) samples at 5 K.

The measurement of temperature dependence magnetic property (M-T curves) under field cooling (FC) with an applied field of 50 Oe and zero field cooling (ZFC) from 5-300 K were performed for Fe_3O_4; Fe_3O_4/ZnS; and Fe_3O_4/ZnS@LaF_3:xCe^{3+},xGd^{3+},yTb^{3+} (x = 5; y = 5, 10 and 15 mol.%) samples. The shape of ZFC/FC curves are more like a collective assemble nanoparticles (NPs). It has been deduced from M-H loops and due to the absence of coercive field. Hence these NPs can be considered as superparamagnetic at room temperature with irreversibility near 300 K. It can be seen the differences between the ZFC profiles for all samples. For Fe3O4 NPs, a maximum can be observed nearly 160 K, indicating its blocking temperature. Further, shifting in blocking temperature can be seen in Fe_3O_4/ZnS (Fig. S3, upper panel) and

Fe_3O_4/ZnS@LaF_3:xCe^{3+},xGd^{3+},yTb^{3+} (x = 5; y = 5 and 15 mol.%) in lower panel of Fig S3 below 300 K. The blocking temperature for sample Fe_3O_4/ZnS@LaF_3:xCe^{3+},xGd^{3+},yTb^{3+} (x = 5; y = 10 mol.%) is not in the measured temperature range. It can be due to dipolar interaction among iron oxide NPs and aggregation of Fe_3O_4/ZnS@LaF_3:xCe^{3+},xGd^{3+},yTb^{3+} (x = 5; y = 10 mol.%) NPs. These changes in blocking temperature also indicate probable random sizes and shapes of materials. It is interesting to notice the magnetization increase on the ZFC and FC curves of the Fe_3O_4/ZnS@LaF_3:xCe^{3+},xGd^{3+},yTb^{3+} (x = 5; y = 5, 10, 15 mol.%) nanomaterials recorded at 2 K, as the temperature further decreases. This effect is due the paramagnetic contribution and considerable magnetic moment of the Tb^{3+} ion, suggesting small effect of Tb^{3+} ion on magnetic properties.

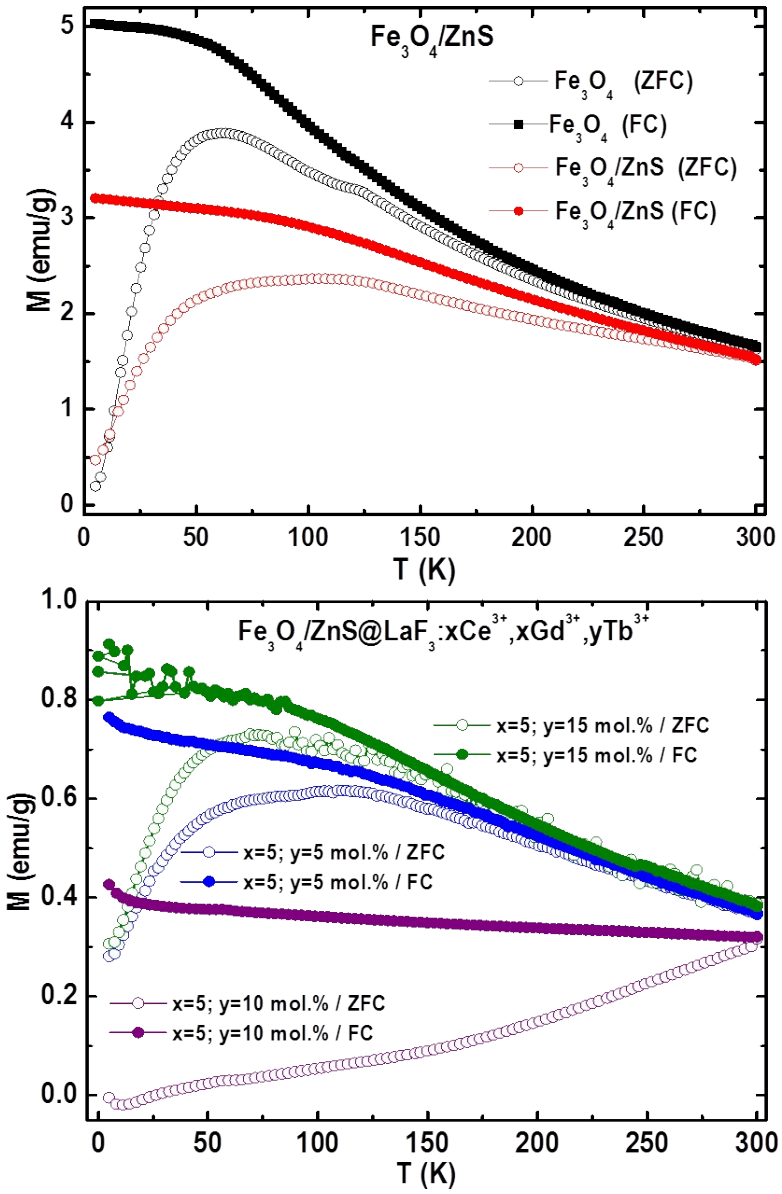

Fig. S3-B: Zero field cooling (ZFC) and Field cooling (FC, at 50 Oe) measurements for the Fe_3O_4 and Fe_3O_4/ZnS (upper panel) and Fe_3O_4/ZnS@LaF_3:xCe^{3+},xGd^{3+},yTb^{3+} (x = 5; y = 5, 10 and 15 mol.%) (lower panel) samples.